Three dimensional-TiO$_2$ nanotube array photoanode architectures assembled on a thin hollow nanofibrous backbone and their performance in quantum dot-sensitized solar cells†

Hyungkyu Han,‡[a] P. Sudhagar,‡[bc] Taeseup Song,[a] Yeryung Jeon,[b] Iván Mora-Seró,[d] Francisco Fabregat-Santiago,[d] Juan Bisquert,[d] Yong Soo Kang*[bc] and Ungyu Paik*[ab]

Facile synthesis of TiO$_2$ nanotube branched (length $\sim$0.5 μm) thin hollow-nanofibers is reported. The hierarchical three dimensional photoanodes (H-TiO$_2$-NFs) (only $\sim$1 μm thick) demonstrate their excellent candidature as photoanodes in QD-sensitized solar cells, exhibiting $\sim$3-fold higher energy conversion efficiency (η = 2.8%, J_{sc} = 8.8 mA cm^{-2}) than that of the directly grown nanotube arrays on a transparent conducting oxide (TCO) substrate (η = 0.9%, J_{sc} = 2.5 mA cm^{-2}).

The mesoscopic sensitized-solar cell is an emerging candidate in electrical power production through direct conversion of solar energy to electrical energy without the greenhouse effect.[1] Recently, quantum dot (QD) semiconductors have attracted a great deal of interest as sensitizers in mesoscopic sensitized solar cells.[2,3] Because of the outstanding abilities in multiple hot carrier generation, panchromatic solar harnessing and high extinction coefficient, the quantum dot-sensitized solar cells (QDSCs) are becoming the future solar energy conversion systems.[4] Many efforts have been invested in developing a wide range of sensitizers; in particular, CdX, PbX, CuInX (X = S, Se, Te) and Ag$_2$S *etc.*, have been tested in QDSCs, resulting in $\sim$4–6% photo conversion efficiency.[5–7] These sensitizers are decorated on a wide band gap metal oxide framework (TiO$_2$, ZnO and SnO$_2$) that acts as a photoanode (selective electron contact). Though QDSCs demonstrate feasible performance utilizing a variety of QD sensitizers, still it requires more improvement to compete with the commercial dye-sensitized solar cells.

Semiconductor QD sensitizers are larger in size than dye molecules; therefore it is difficult to penetrate deeper parts of

TiO$_2$ electrodes, thus limiting the sensitizer loadings. Although, the higher extinction coefficient of semiconductor QDs, in comparison with molecular dyes, partially compensates for the loss of the effective surface area and subsequently the decrease in the sensitizer loading, configuring the photoanode framework with a large-pore network is necessary to further promote the QD sensitizer loading.[8] In addition, such photoanodes could demonstrate high charge transport from the sensitizer to a charge collector, ultimately overwhelming the charge recombination at the photoanode/electrolyte interface. Thus, to achieve high sensitizer loading, fast electron transport channel, and good electrolyte pore-filling, establishing vertically aligned nanostructures, in particular, directly synthesized on transparent conductive oxides (TCO), has been identified as the promising approach in dye or QD-sensitized solar cells.[9] Most importantly, vertically grown nanotube (NT) arrays have longer electron diffusion length and more benefits in pore-filling of solid state hole transport materials (HTM), compared to disordered TiO$_2$ mesoporous films.[10] Diverse methods were demonstrated for the fabrication of TiO$_2$ NT arrays, including electrochemical anodization,[11] hydrothermal treatment[12] and vapour–liquid–solid methods. Recently, the Gao group developed directly assembled TiO$_2$ NT arrays on TCO using ZnO nanowire templates.[13] Though direct assembly of NT arrays on TCO substrates is more adventurous,[14] template-based NT arrays have wide tube–tube voids which resulted in less distribution compared to the anodization technique. Besides, such low density of NTs on a TCO substrate markedly lowers the internal surface area of the electrode as well as limits the QD loading.

One simple way to promote the interface surface area of the NT array is to extend its length,[15] however there exists a trade-off between the NT length and mechanical stability. Therefore, assembling NT arrays on a highly interconnected 3D fibrous backbone would be a more effective way to achieve high electron transport channels in energy conversion devices.[16–18] Scheme 1 illustrates the fabrication stages of hierarchical 3-D hollow TiO$_2$ nanofibers (H-TiO$_2$-NFs). Our proposed hierarchical 3-D hollow TiO$_2$ NFs would be the optimum nanostructure for achieving higher sensitizer loading and fast electron transport for QDSCs. In this communication, we demonstrate the fabrication of TiO$_2$ nanotubes branched on

[a] *Department of Materials Science & Engineering, Hanyang University, Seoul 133791, South Korea*

[b] *World Class University Program Department of Energy Engineering, Hanyang University, Seoul 133791, South Korea. E-mail: upaik@hanyang.ac.kr*

[c] *Center for Next Generation Dye-Sensitized Solar Cells, Hanyang University, Seoul 133791, South Korea. E-mail: kangys@hanyang.ac.kr*

[d] *Photovoltaics and Optoelectronic Devices Group, Departament de Física Universitat Jaume I, 12071 Castelló, Spain*

† Electronic supplementary information (ESI) available: Experimental and characterization details. See DOI: 10.1039/c3cc40439k
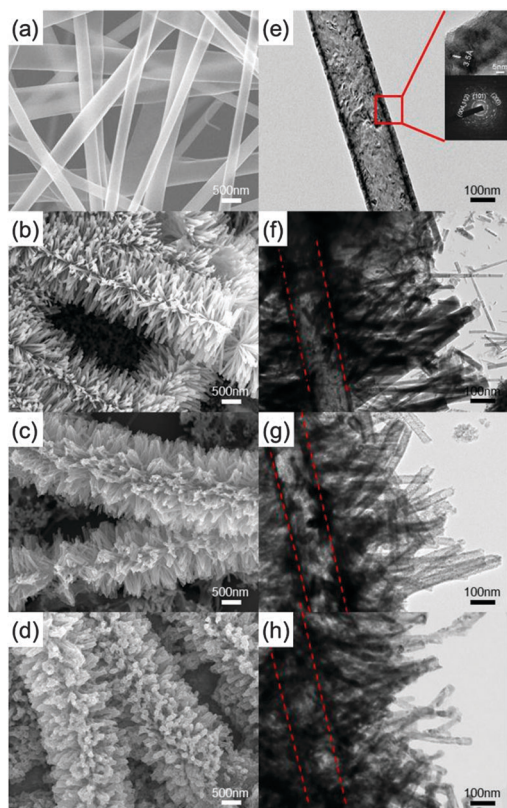
‡ These authors contributed equally to this research.
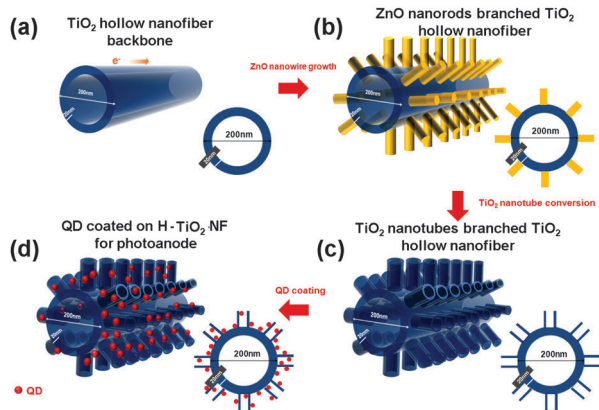
Scheme 1 Schematic illustration of H-TiO$_2$ NF photoanode fabrication stages of (a) TiO$_2$ hollow nanofibers (TiO$_2$-NFs), (b) ZnO NR templates grown on TiO$_2$-HNFs, (c) TiO$_2$ nanotube branches grown on TiO$_2$-NFs through ZnO NR templates, and (d) QD-sensitized H-TiO$_2$ NF photoanode.

TiO$_2$ hollow nanofiber photoanodes, directly grown on TCO, and elucidate their candidature as an excellent photoanodes in QDSCs.

Fig. 1a shows the scanning electron microscopy (SEM) image of backbone TiO$_2$ NFs confirming the continuous 1D geometry. The distribution of the fiber diameter lies between 200 and 500 nm with an average wall thickness of 20 nm. The ZnO NR templates with an average diameter of ∼25 nm and a length of ∼500 nm were vertically grown on the 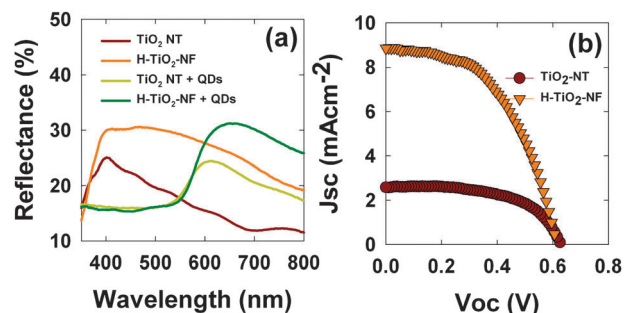outer surface of TiO$_2$ NFs which completely covered the backbone (Fig. 1b). After coating the TiO$_2$ thin layer on ZnO NRs, the ZnO templates were finally removed by selective etching (Fig. 1c). Fig. 1d shows the QD-sensitized 3-D TiO$_2$ nanotubes branched on TiO$_2$ hollow nanofibers (H-TiO$_2$ NFs). The high resolution TEM images and the selective area electron diffraction (SAED) pattern reveal that the TiO$_2$ hollow nanofibers possess an anatase phase and polycrystalline nature (Fig. 1e). Fig. 1(f) reveals that the spatially decorated ZnO NT arrays on TiO$_2$ NFs have good contact with the TiO$_2$ backbone. Furthermore, TEM images (Fig. 1g and h) suggest that the TiO$_2$ tubular branches have sufficiently large pore channels for electrolyte filling as well as good structural stability even after removing the ZnO templates and QD sensitization, respectively.

The detailed experimental procedure for the fabrication of hierarchical TiO$_2$ NFs, QD sensitization (CdS/CdSe with a ZnS passivation layer) and QDSC device fabrication steps is explained in the ESI† (see SA and SB). To demonstrate the influence of electrode geometry on photovoltaic performance of QDSCs, the following electrodes were tested as photoanodes in QDSCs: (a) directly grown TiO$_2$ NTs on TCO (TiO$_2$-NT) and (b) hierarchical three dimensional TiO$_2$ nanotubes branched on hollow TiO$_2$ NF (H-TiO$_2$ NF) electrodes. The optical reflection capability of both TiO$_2$-NTs and H-TiO$_2$ NFs is studied by diffused reflectance spectra (Fig. 2a). Under the identical TiO$_2$ nanotube growth conditions, the H-TiO$_2$ NF electrodes show high reflectance compared to TiO$_2$-NTs in the wavelength range of 380–800 nm. This might be attributed to the multiple scattering of incident light at the hierarchical TiO$_2$ NT branches, thus drastically enhancing the reflectance of the electrode. Both QD-sensitized TiO$_2$-NT and H-TiO$_2$ NF electrodes found to exhibit decreased reflectance at wavelengths 610 and 660 nm, respectively, due to the light absorption of the CdS/CdSe sensitizer.

By subtracting the electrode effect from QD-sensitized TiO$_2$ samples, we estimated the optical reflectance of only QDs (-DR) (see ESI,† SD). From Fig. S3 (ESI†), a high -DR was observed at H-TiO$_2$-NFs, which evinces the higher loading of QDs compared to TiO$_2$-NT electrodes. The photovoltaic performance (J–V plots) of TiO$_2$-NT and H-TiO$_2$ NF photoanodes are presented in Fig. 2b and the estimated PV parameters are summarized in Table 1.

The TiO$_2$-NTs directly grown on a FTO electrode resulted in a photoconversion efficiency (PCE) of ca. η = 0.9% with photovoltage, V_{oc} = 0.62 V, photocurrent, J_{sc} = 2.5 mA cm^{-2} and fill factor, FF = 58.3%. As anticipated, the hierarchical TiO$_2$ nanotube branches grown on a hollow NF backbone show unprecedentedly promoted

Fig. 1 FE-SEM images (a–d) and HR-TEM images (e–h) of TiO$_2$ hollow nanofibers, ZnO nanorods branched on TiO$_2$ hollow nanofibers, TiO$_2$ nanotubes branched on TiO$_2$ hollow nanofibers, and QD-sensitized 3-D TiO$_2$ nanotubes branched on TiO$_2$ hollow nanofibers respectively.

Fig. 2 (a) Reflectance spectra of bare and QD-sensitized TiO$_2$ nanostructured electrodes, (b) J–V plots of QDSCs using different photoanodes (electrode thickness: ∼1 µm, device active area: 0.25 cm^{-2} without mask, electrolyte: 1 M polysulfide and counter electrode: nanocarbon black).

Table 1 Photovoltaic parameters of QDSCs using different photoanodes

Photoanode	V_{oc} (V)	J_{sc} (mA cm^{-2})	FF (%)	Efficiency (%)
TiO$_2$-NT	0.62	2.5	58.3	0.9
H-TiO$_2$ NF	0.61	8.8	50.3	2.8
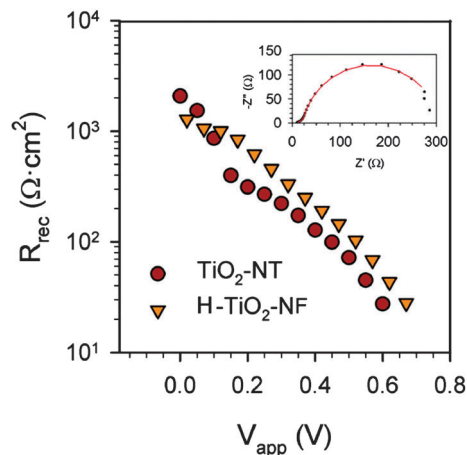
Fig. 3 Recombination resistance of TiO$_2$-NT and H-TiO$_2$ NF QDSCs. The inset shows Nyquist plots of the H-TiO$_2$ NF sample at applied voltage, V_{app} = 0.57 V. The red solid line is the fit of the experimental data points using the previously described model for EIS analysis of QDSC samples.[7]

PCE to η = 2.8% with V_{oc} = 0.61 V, J_{sc} = 8.8 mA cm^{-2} and F.F. = 50.3%. It is clearly evident that the TiO$_2$ NTs spatially assembled on the hierarchical 3D-nanofibrous backbone promote the QDSC performance by a factor of three compared to the TiO$_2$ NTs directly grown on a TCO substrate. We can relate the enhancement of photocurrent generation with the H-TiO$_2$ NF photoanodes to several contributions: (a) higher effective surface area and consequently higher QD loading and light harvesting; (b) highly efficient charge collection throughout the photoanode with fewer boundary layers and (c) the multiple scattering effect of the comb-like hierarchical NT arrays, in particular, red photon harvesting (see ESI,† SE and Fig. S4).

On the other hand, it is interesting to point out that V_{oc} values obtained for both devices are similar, in spite of the larger effective surface area of H-TiO$_2$ NFs, for which a higher recombination rate (and consequently lower V_{oc}) is expected. But this is not the case as observed in Fig. 2b, where similar V_{oc} values are observed for both the samples. For further understanding of this behaviour, the QDSC recombination has been analyzed using the electrochemical impedance spectroscopy (EIS). The stability of the samples during the impedance measurement was verified by comparing the cyclic voltammograms before and after EIS measurement (see ESI,† SF and Fig. S5). Fig. 3 shows the recombination resistance obtained for the samples analyzed in Fig. 2b. Similar recombination resistances are observed for both samples. Despite the larger effective surface area of H-TiO$_2$ NFs, the recombination resistance does not become significantly higher than the resistance observed for TiO$_2$-NTs.

In this sense, the recombination rate does not increase for the hierarchical sample; rather it decreases as shown in Fig. 3. This may contribute to the significant 3-fold enhancement in the solar cell efficiency observed for the H-TiO$_2$ NFs in comparison with the TiO$_2$-NTs. The huge increase in photocurrent is not deleteriously compensated by a reduction in V_{oc}, giving place for a final efficiency

improvement of 310%. In addition, high collection efficiency can be deduced for H-TiO$_2$ NF QDSCs (see ESI,† SG and Fig. S6).

In summary, 3-D hierarchical TiO$_2$ nanotube branches were successfully assembled onto the primary hollow TiO$_2$ nanofibrous backbone. The newly designed H-TiO$_2$ NF photoanode offered large surface area for high QD loading with high light scattering property. In comparison with the NT arrays directly grown on a TCO substrate, the introduction of NTs on the continuous hollow nanofibrous layer results in effective charge collection. In addition, the hierarchical structure enhances effective surface area without altering the recombination rate, as should be expected. The proposed H-TiO$_2$ NF architecture fabricated using the simple protocol can allow wide applications in electrochemical energy conversion and storage devices including QDSCs, DSSCs, photocatalysts and batteries, where highly catalytic/electroactive materials have to be loaded and fast charge transport characteristics are required.

Notes and references

1 A. Yella, H. W. Lee, H. N. Tsao, C. Y. Yi and A. K. Chandiran, *Science*, 2011, **334**, 1203.
2 I. Mora-Sero and J. Bisquert, *J. Phys. Chem. Lett.*, 2010, **1**, 3046–3052.
3 P. V. Kamat, *J. Phys. Chem. C*, 2008, **112**, 18737–18753.
4 S. Ruhle, M. Shalom and A. Zaban, *ChemPhysChem*, 2010, **11**, 2290–2304.
5 A. Braga, S. Gimenez, I. Concina, A. Vomiero and I. Mora-Sero, *J. Phys. Chem. Lett.*, 2011, **2**, 454–460.
6 P. K. Santra and P. V. Kamat, *J. Am. Chem. Soc.*, 2012, **134**, 2508–2511.
7 V. Gonzalez-Pedro, X. Q. Xu, I. Mora-Sero and J. Bisquert, *ACS Nano*, 2010, **4**, 5783–5790.
8 M. Samadpour, S. Gimenez, P. P. Boix, Q. Shen, M. E. Calvo, N. Taghavinia, A. I. Zad, T. Toyoda, H. Miguez and I. Mora-Sero, *Electrochim. Acta*, 2012, **75**, 139–147.
9 K. Zhu, N. R. Neale, A. Miedaner and A. J. Frank, *Nano Lett.*, 2007, **7**, 69–74.
10 J. Bandara, K. Shankar, J. Basham, H. Wietasch, M. Paulose, O. K. Varghese, C. A. Grimes and M. Thelakkat, *Eur. Phys. J.: Appl. Phys.*, 2011, **53**, 20601.
11 J. Wang and Z. Q. Lin, *J. Phys. Chem. C*, 2009, **113**, 4026–4030.
12 H. H. Ou and S. L. Lo, *Sep. Purif. Technol.*, 2007, **58**, 179–191.
13 C. K. Xu, P. H. Shin, L. L. Cao, J. M. Wu and D. Gao, *Chem. Mater.*, 2010, **22**, 143–148.
14 P. Chen, J. Brillet, H. Bala, P. Wang, S. M. Zakeeruddin and M. Gratzel, *J. Mater. Chem.*, 2009, **19**, 5325–5328.
15 C. K. Xu and D. Gao, *J. Phys. Chem. C*, 2012, **116**, 7236–7241.
16 M. Shang, W. Z. Wang, W. Z. Yin, J. Ren, S. M. Sun and L. Zhang, *Chem.–Eur. J.*, 2010, **16**, 11412–11419.
17 N. Tetreault, E. Horvath, T. Moehl, J. Brillet, R. Smajda, S. Bungener, N. Cai, P. Wang, S. M. Zakeeruddin, L. Forro, A. Magrez and M. Gratzel, *ACS Nano*, 2010, **4**, 7644–7650.
18 P. Sudhagar, V. Gonzalez-Pedro, I. Mora-Sero, F. Fabregat-Santiago, J. Bisquert and Y. S. Kang, *J. Mater. Chem.*, 2012, **22**, 14228–14235.